AIAA JOURNAL
Vol. 40, No. 1, January 2002

Turbulence Ingestion Noise, Part 2: Rotor Aeroacoustic Response to Grid-Generated Turbulence

John P. Wojno* and Thomas J. Mueller†
University of Notre Dame, Notre Dame, Indiana 46556
and
William K. Blake‡
U.S. Naval Surface Warfare Center, West Bethesda, Maryland 20817-5700

This is the second of two papers that discuss an experimental investigation of the aeroacoustic response characteristics of a 10-bladed rotor to grid-generated turbulence. To characterize empirically the rotor response, both the ingested velocity field and resulting far-field sound were measured. In part 1, an empirical velocity characterization of the grid- generated turbulence field was presented. This characterization culminated in a semi-empirical model of the ingested small-scale turbulence field and a modal decomposition of the circumferentially varying mean velocity field in the rotor inlet plane. This detailed velocity model is now used to investigate the aeroacoustic response of a 10-bladed rotor ingesting the grid-generated turbulence field. In particular, the semi-empirical turbulence model is used, in conjunction with theoretical spectral analysis techniques, to predict the far-field sound generated by the 10-bladed rotor. These predictions are compared to corresponding measured data to assess the fidelity of the spectral analysis methods and the semi-empirical turbulence model. Finally, the measured 10-bladed acoustic response is compared to the corresponding response of a 4-bladed rotor ingesting the same grid-generated turbulence field. These comparisons demonstrate the effect of geometry on the rotor aeroacoustic sensitivity to both large-scale, spatial mean velocity modes and small-scale turbulence.

Nomenclature

$A(k_{12}b)$	=	tangential wave number filtering function, as defined in Eq. (8)
B	=	number of rotor blades
b	=	rotor blade spacing
c	=	rotor blade chord
c_0	=	speed of sound in the ambient fluid
f	=	temporal frequency
f_{TE}	=	frequency at which trailing-edge effects become important
$G(\boldsymbol{k}, f)$	=	unsteady aerodynamic response function
$H(f)$	=	acoustic propagation model
$\boldsymbol{k}$	=	wave vector
k_0	=	acoustic wave number
k_1	=	streamwise wave number
k_2	=	wave number normal to the blade
k_{12}	=	composite wave number along rotation direction
L_R	=	rotor blade span (defined from hub to tip)
M	=	Mach number
m	=	mesh spacing
n	=	circumferential harmonic mode number of mean velocity field
R	=	radial location in rotor plane
R_{tip}	=	rotor tip radius
$\hat{R}_{TT}(\tau)$	=	correlated rotor thrust response
r_s	=	acoustic receiver/source range
$Se(k_1c/2)$	=	Sears's unsteady aerodynamic response function
s_{grid}	=	solidity of turbulence generation grid
t	=	rotor blade thickness
U_{mean}	=	measured mean flow velocity
$U_0(R)$	=	resultant mean flow velocity (in the rotating reference frame)
U_∞	=	freestream mean flow velocity
$\underline{u_i}$	=	velocity fluctuation in the ith direction
$\overline{u^2}$	=	mean-squared turbulence velocity
V_c	=	convection velocity
$\boldsymbol{x}$	=	vector location of acoustic receiver
$\boldsymbol{y}$	=	vector location of acoustic source
β	=	acoustic receiver/source azimuth angle, measured with respect to the dipole axis
δ_{TE}	=	empirically estimated boundary layer thickness at blade trailing edge
δ_{theory}	=	theoretical boundary-layer thickness estimate, based on Schlicting's analysis
η_i	=	cosine describing the ith direction
Λ_i	=	turbulence length scale in ith direction
ρ	=	fluid density
$\Phi_{PP}(f)$	=	measured far-field acoustic pressure spectrum
$\tilde{\Phi}_{PP}(f)$	=	estimated far-field acoustic pressure spectrum
$\Phi_{TT}(f)$	=	unsteady thrust spectrum
$\Phi_{uu}(\boldsymbol{k})$	=	three-dimensional turbulent wave number spectrum
$\phi(k_i)$	=	nondimensional, spectral density in the ith direction wave number domain
Ω	=	angular rotation rate

Subscript

θ	=	tangential component

Received 6 December 1999; revision received 1 June 2001; accepted for publication 11 June 2001.

*Research Assistant, Aerospace and Mechanical Engineering Department; currently Acoustic Engineer, Hydroacoustics, U.S. Naval Surface Warfare Center, Carderock Division, Code 7250, West Bethesda, MD 20817-5700.

†Roth-Gibson Professor, Aerospace and Mechanical Engineering Department. Associate Fellow AIAA.

‡Chief Scientist, Hydroacoustics, Carderock Division, Code 7023.

I. Introduction

THE historical background for these experiments was presented in greater detail in part 1 of this paper.[1] However, it is important to remember that this investigation was a modern extension of the pioneering work of Sevik.[2] The desire for dynamic similarity with this earlier work influenced the definition of the experimental test conditions, as outlined in Sec. III. The theoretical analysis, however, which is presented in Sec. II, was performed in the spectral domain, in the manner of Blake,[3] as opposed to the spatial domain analysis originally used by Sevik.[2]

Rotor turbulence ingestion noise (TIN) has been a previous topic of investigation at Notre Dame. Scharpf[4] and Minniti et al.[5] measured the aeroacoustic response of a four-bladed rotor to grid-generated turbulence. However, the velocity data in these studies were limited to the classical turbulence parameters, such as the rms turbulence intensity, the Lagrangian integral scale, and the temporal autospectrum. Furthermore, the blade spacing of the four-bladed rotor was very large with respect to the measured turbulence scales.

The major objectives for the current research effort were to fully characterize the ingested velocity field, to investigate the effect of rotor geometry on the aeroacoustic response, and to assess the fidelity of spectral analysis prediction techniques for estimating the rotor TIN. The first objective was accomplished through a detailed series of velocity measurements in the rotor inlet plane. This portion of the current research was presented in part 1 of this paper.[1] The second objective was accomplished by comparing the far-field acoustic emissions from two different geometry rotors operating downstream of the turbulence generation grids.

The specific rotor geometries used for these experiments were selected to facilitate comparisons to prior TIN studies.[2,4,5] Martinez's results[6] provided the motivation for selecting the primary rotor geometry. As noted earlier, his theoretical analysis suggested that Sevik's empirical thrust data[2] overestimated the rotor response at the higher harmonics of the blade passing frequency (BPF). To investigate this possibility, Sevik's 10-bladed rotor was selected as the primary focus of the current testing. Previous TIN studies at Notre Dame have populated an extensive empirical database that defines the aeroacoustic response a four-bladed rotor to turbulence generated by the same grids that were used here. Consequently, the 4-bladed rotor geometry was selected for comparison to the 10-bladed rotor. Furthermore, because the response characteristics of the four-bladed rotor to the grid-generated turbulence field were quantified in great detail by the previous investigators, only limited noise measurements were made with the four-bladed rotor in this study, as necessary for direct comparisons between the two geometries. Rather, the current experiments focused on measuring the acoustic response of the 10-bladed rotor to the ingested velocity field. Comparisons between the response characteristics of both rotors demonstrated the geometric dependence of the rotor aeroacoustic sensitivity to large-scale, spatial mean velocity gradients and small-scale turbulence.

The final research objective was achieved by estimating the broadband acoustic response of the primary rotor geometry and comparing the predicted sound levels to the corresponding measured data. The detailed velocity characterization presented in part 1 of this paper,[1] coupled with the measured far-field sound levels presented later, comprised a comprehensive definition of the 10-bladed rotor broadband response to the ingested turbulence field. For comparison to the measured data, the previously developed semi-empirical turbulence model[1] was used to define inputs to a theoretical aeroacoustic response model, based on the spectral analysis methods of Blake,[3] to generate corresponding theoretical predictions of the TIN from the 10-bladed rotor. The methodology for the assessment is shown graphically in Fig. 1. In this manner, the spectral analysis techniques were evaluated in terms of their ability to predict the measured sound levels.

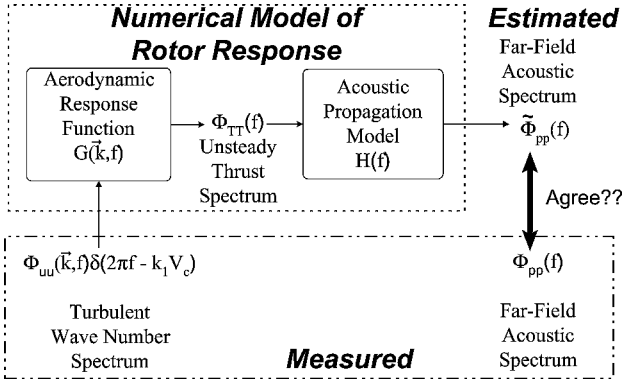

Fig. 1 Functional block diagram of the comparisons between the predicted and measured responses.

II. TIN Predictions

The theoretical analysis tools that were required to estimate the rotor TIN are presented in the following sections. These analyses are presented in a functional manner and start with the far-field acoustic propagation law. This equation relates the far-field sound pressure to the rotor unsteady thrust. This is followed by the unsteady aerodynamic response model, which was used to estimate the rotor unsteady thrust spectrum in terms of the spectral content of the ingested turbulence field. Because of space and time constraints, only the highlights of the theory are presented here. Detailed derivations of the theoretical analysis were presented by Wojno.[7]

A. Acoustic Propagation Law

The rotor was acoustically modeled as a compact dipole whose axis is aligned with the axis of rotation. Therefore, the amplitude of the acoustic pressure spectrum at a point $\boldsymbol{x}$ in the far field is directly related to the amplitude of the unsteady thrust spectrum[3]:

$$|\Phi_{PP}(\boldsymbol{x}, f)| = \left(\frac{k_0 \cos\beta}{4\pi r_s}\right)^2 |\Phi_{TT}(f)| \tag{1}$$

The fidelity with which this simple approximation captured the associated physical phenomena is evaluated in Sec. IV.B by comparing the measured far-field sound emitted from the 10-bladed rotor with the corresponding predictions based on Eq. (1).

B. Unsteady Aerodynamic Response

As shown in Eq. (1), the unsteady thrust spectrum was required to estimate the far-field noise. By definition, the unsteady thrust response is the integrated effect of the local aerodynamic response of the rotor blades to the spatiotemporal turbulent disturbance. Because of the relative simplicity of the primary rotor geometry (constant chord with zero sweep), aerodynamic strip theory was used to approximate the unsteady thrust response of the rotor in terms of the local behavior of radial blade sections, assuming constant behavior across each section. However, to estimate properly the levels of the local blade response, the analysis was performed in a blade-fixed, rotating reference system, in which the local convection velocity was defined as follows:

$$V_c \equiv U_0(R) = \sqrt{U_\infty^2 + (\Omega R)^2} \tag{2}$$

Furthermore, the following simplifying assumptions were made: the flow is locally two dimensional; viscous effects are negligible; the flow is incompressible (because $M \approx 0.03 \ll 1$); the rotor comprises thin, unloaded airfoils; the turbulent disturbances act normal to the blade and are small compared to the mean velocity; and the rotor solidity is small enough to ignore cascade, that is, blade interaction, effects over the frequency range of interest.

Based on these assumptions, Sears's unsteady aerodynamic response function was used to estimate the aerodynamic response of each radial blade section, based on the local blade geometry and flow parameters. Consequently, the estimated temporal radial thrust distribution for a given radial section of the sth blade to the turbulence component $u(\boldsymbol{k}, f)$ was given by Eq. (3). Note that neglection of the rotor solidity effects may have resulted in discrepancies between the predicted and measured sound levels at low frequencies ($f < 0.7$ BPF), as shown in Sec. IV.B:

$$\frac{\mathrm{d}T_s}{\mathrm{d}R}(R,t) = \eta_i(R)\left\{\pi\rho c u(\boldsymbol{k}, f) U_0(R) \times Se\left(\frac{k_1 c}{2}\right) \times \exp[i(k_R R - 2\pi f t)]\exp(ik_{12} s b)\right\} \tag{3}$$

The temporal thrust response of the sth blade due to $u(\boldsymbol{k}, f)$ was obtained by integrating Eq. (3) over the radius. Therefore, the temporal thrust response of the rotor was estimated by simply summing the contributions from all of the blades:

$$T(t) = \sum_{s=0}^{B-1}\left[\int_{R_{\text{hub}}}^{R_{\text{tip}}} \frac{\mathrm{d}T_s}{\mathrm{d}R}(R,t)\,\mathrm{d}R\right] \tag{4}$$

However, turbulence, by its nature, is nondeterministic, and so it is customary to work with the spectral response in turbulence applications. Furthermore, the primary parameter of interest in aeroacoustics is the acoustic power, which is directly related to the mean-squared pressure. The acoustic propagation law presented in Eq. (1) relates the acoustic pressure spectrum (or, equivalently, mean-squared acoustic pressure) at a point in the far field to the unsteady thrust spectrum (or mean-squared unsteady thrust). Therefore, the primary aerodynamic response parameter relevant to the far-field sound was the unsteady thrust spectrum. Consequently, an expression was developed to estimate the unsteady thrust spectrum $\Phi_{TT_i}(f)$ in terms of the wave number spectrum $\Phi_{uu}(\boldsymbol{k})$ of the ingested turbulence. By definition, the unsteady rotor thrust spectrum $\Phi_{TT}(f)$ is the temporal Fourier transform of the correlated thrust response:

$$\Phi_{TT}(f) = \frac{1}{2\pi}\int_{-\infty}^{\infty} \exp(i2\pi f\tau)\hat{R}_{TT}(\tau)\,\mathrm{d}\tau \tag{5}$$

The correlated rotor thrust is defined in terms of the temporal rotor thrust response, as given by Eq. (4):

$$\hat{R}_{TT}(\tau) = \langle T(\boldsymbol{y}, t),\, T(\boldsymbol{y}, t+\tau)\rangle \tag{6}$$

In addition, the following assumptions were made about the ingested turbulence field: the turbulence is homogeneous; the three-dimensional turbulent wave number spectrum can be modeled as a separable function, the radial turbulence length scale is smaller than the rotor blade span ($\Lambda_R/L_R \ll 1$), the turbulence length scales are functions of the streamwise wave number k_1, and Taylor's hypothesis is valid. The first two assumptions were made to make the analysis tractable. However, the velocity field was shown to be inhomogeneous in part 1 of this paper.[1] To account for modulation of the ingested turbulence due to inhomogeneity, a scaled near-isotropic turbulence model was defined in terms of the measured spatial averages of the relevant turbulence characteristics. Although the directional separability assumption might initially seem to be excessively restrictive, the measured turbulent cross-spectral density demonstrated an equivalent directional independence in part 1. Finally, the latter three assumptions were also shown to be reasonable in the previous publication.

Given these simplifying assumptions, an expression was defined for the unsteady thrust spectrum in terms of the ingested turbulence spectrum, based on Eqs. (5) and (6). The details of the derivation are too extensive for inclusion here, and so only the result is presented in Eq. (7) (see Wojno[7] for a detailed derivation). Note that use of the Sears function to define the sectional response required that the turbulent excitation be referenced to the local, blade-fixed coordinate system, as outlined in part 1:

$$\Phi_{TT_i}(f) = \int_{-\infty}^{\infty}\left\{\int_{R_{\mathrm{hub}}}^{R_{\mathrm{tip}}} \pi^2\rho^2c^2\left|Se\left(\frac{k_1c}{2}\right)\right|^2\left(\frac{2\Lambda_R(k_1)}{L_R}\right)\right.$$
$$\left.\times\, U_0^2(R)\eta_i^2(R)\Phi_{uu}(k_1)\left[\int_{-\infty}^{\infty}|A(k_{12}b)|^2\phi(k_2)\,\mathrm{d}k_2\right]\mathrm{d}R\right\}\delta[2\pi f$$
$$-\,k_1U_0(R)]\,\mathrm{d}k_1 = \int_{-\infty}^{\infty}\Phi_{TT_i}(k_1)\delta[2\pi f - k_1U_0(R)]\,\mathrm{d}k_1 \tag{7}$$

where

$$A(k_{12}b) = \sum_{s=0}^{B-1}\exp(ik_{12}sb)$$
$$= \frac{\sin[(B/2)k_{12}b]}{\sin\left(\frac{1}{2}k_{12}b\right)}\exp\left[i(B-1)\left(\tfrac{1}{2}k_{12}b\right)\right] \tag{8}$$

The integration over the blade-normal wave number k_2 that is enclosed in square brackets in Eq. (7), is a very important parameter. This component defines the degree of blade-to-blade correlation in the rotor response.[3,7] It accounts for the coherent portion of the blade–disturbance interaction over the entire rotor. If the blade spacing is much larger than the tangential turbulence scale ($\Lambda_\theta/b \to 0$), the individual blade responses are uncorrelated. When this happens, each blade interacts independently with the disturbance. Consequently, the summation gain $A(k_{12}b)$ is constant at all frequencies and equal to the number of rotor blades B, and the rotor response is said to be incoherent. Furthermore, the incoherent response is strictly broadband. However, when the turbulence scale is large enough to interact with multiple blades ($\Lambda_\theta > b$), the summation gain generates a series of sidebands in wave number space, as shown in Fig. 2. These sidebands are convolved with the tangential turbulence spectral density and integrated over k_2 in Eq. (7), to generate narrowband features about the BPF and higher harmonics, similar to the haystacks predicted by Martinez.[6,8,9] The amplitude of these peaks depends on the number of blades that simultaneously interact with a given disturbance. Blake showed[3] that, in the asymptotic limit of perfect correlation ($\Lambda_\theta/b \to \infty$), the amplitude of the summation gain about the BPF and higher harmonics goes to B^2. For most physical TIN problems, the value of the summation gain lies between these two extremities.

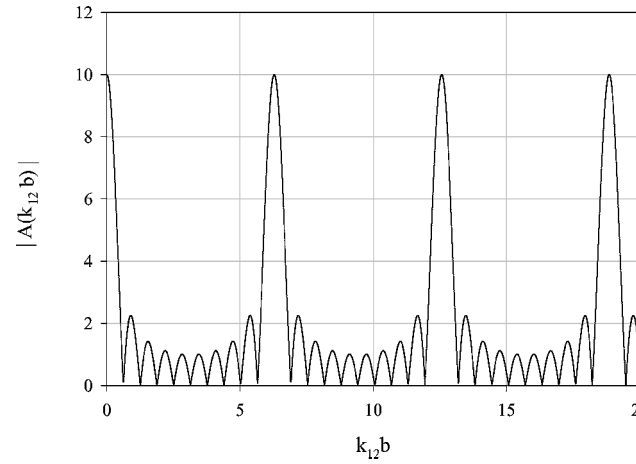

Fig. 2 Sidebands generated by rotor summation gain.

III. Definition of Experiment

A. Facility

All of the experiments in the current study were performed in the anechoic wind tunnel (AWT) facility at the Hessert Center for Aerospace Research at Notre Dame. This facility is a 61-cm (2-ft) square, freejet, indraft wind tunnel, enclosed in an anechoic chamber. The tunnel has a nominal mean velocity range of 5–33 m/s and a nominal freestream turbulence intensity at the jet centerline of 0.08% at exit of the inlet, or about 0.2% at the test location. The low-frequency cutoff of the anechoic chamber is approximately 100 Hz. A motorized rotating boom is suspended at the center of the test section from which microphones can be suspended to measure the far-field acoustic radiation. The current configuration allows accurate acoustic measurements over an arc of approximately 90 deg, centered at the midplane of the test section. Additional information about the AWT facility is given by Mueller et al.[10]

B. Test Conditions

As outlined in part 1 of this paper,[1] the basic flow parameters were selected to maximize dynamic similarity with the work of Sevik,[2] while operating at the same mean flow conditions as the previous TIN studies at Notre Dame. All of the current data were collected at a mean freestream velocity of 12.7 m/s (41.9 ft/s), which was the flow speed at which the majority of the previous four-bladed response data were taken.[4,5,11] Three different rectangular turbulence generation grids were used, each with a different mesh spacing, $m = 1.905$, 3.175, and 7.62 cm (0.75, 1.25, and 3.0 in.), and rod diameter, $d = 0.3175$, 0.635, and 1.27 cm (0.125, 0.25, and 0.5 in.), respectively. The resulting grid solidities ($s_{\mathrm{GRID}} = 0.26$, 0.34, and 0.33) were nominally equal to that of the grids used by Sevik ($s_{\mathrm{Sevik}} = 0.26$ and 0.34) (Ref. 2).

The rotor inlet plane was defined to be approximately 61 cm (24 in.) downstream of the grids, which corresponded to the

Table 1 Test conditions for 10-bladed rotor nominal mean flow velocity: 12.7 m/s (41.9 ft/s)

Case	Ω, rpm	BPF, Hz	J
1	2400	400	1.56
2	2880	480	1.31
3	3300	550	1.14

Table 2 Test conditions for four-bladed rotor nominal mean flow velocity: 12.7 m/s (41.9 ft/s)

Ω, rpm	BPF, Hz	J
2400	160	1.25
2880	192	1.04
3300	220	0.91

midpoint of the test section. The rotor acoustic tests were performed with the rotors turning downstream of the grids at 2400, 2880, and 3000 rpm. These rotation rates, coupled with the specified mean flow velocity, resulted in the corresponding BPF and advance coefficient J values presented in Tables 1 and 2, for the 10-bladed and 4-bladed rotors, respectively. The acoustic measurements for both rotors at the all of the test conditions were made at a single locations in the far field, 0.9 m (36 in.) from the rotor, along an angle $\beta = 45$ deg, measured with respect to the upstream axis of rotation (the tunnel centerline). This particular location was selected because it was the point in the anechoic region of the tunnel that provided the maximum acoustic signal amplitude.[7]

IV. Acoustic Response Characterization

As noted earlier, one of the primary objectives of this research was to predict the broadband response of a rotor to the grid-generated turbulence field. Consequently, a theoretical analysis was developed in Sec. II, which predicts the aeroacoustic response of the rotor to the spectral content of the ingested turbulence field. Furthermore, a semi-empirical spectral density model was developed in part 1 of this paper, based on the spatial averages of the relevant measured turbulence characteristics, which accounted for the large-scale, spatial modulation of the fine-scale turbulence.[1] This semi-empirical turbulence model was used to define a representative small-scale turbulence disturbance for the TIN predictions. The broadband acoustic response of the 10-bladed rotor to the semi-empirical turbulence model was estimated using a numerical program (written in MATLAB® language, version 5.0), based on the analysis developed in Sec. II.

Corresponding experiments were performed to measure the far-field sound emitted by the 10-bladed rotor due to the ingested turbulence field. These data are presented in Sec. IV.B. In addition to the 10-bladed acoustic data, the corresponding acoustic production of a 4-bladed rotor ingesting the same turbulence field was also measured. These data were used to demonstrate the effect of geometry on the rotor aeroacoustic response to the ingested velocity field, as shown in Sec. IV.C.

The error propagation method of Kline and McClintock (see Ref. 12) was used to estimate the uncertainty in the measured sound pressure level (SPL). This analysis, which was presented in greater detail by Wojno,[7] gave an overall uncertainty in the measured SPL of ± 0.5 dB referenced to 20 μPa. Because this uncertainty was a only function of the measurement equipment, this uncertainty applies to all of the measured SPL data. The uncertainty associated with the measured velocity data is presented in part 1 of this paper.[1]

A. Isolating the Measured Rotor Acoustics

To assess the acoustic emissions due to the rotor, comparisons were made between the acoustics measured with the rotor operating and the corresponding tunnel background noise. The background noise level was measured with the grid mounted in the tunnel, at the specified mean flow velocity, without the rotor operating. Sample comparisons of the grid and rotor plus grid noise levels, for the 10-bladed rotor operating at test cases 2 and 3, are presented in Fig. 3.

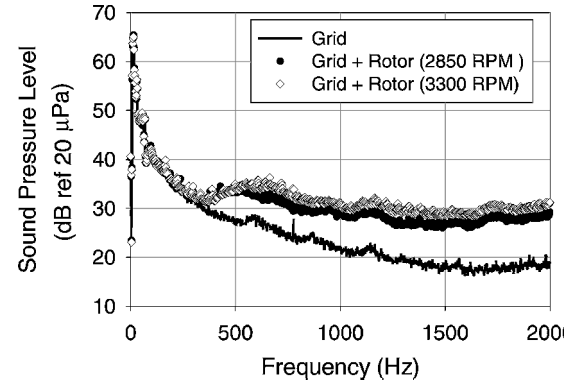

Fig. 3 Measured SPL with 10-bladed rotor, relative to background, rotor located 61 cm (24 in.) downstream of 7.62-cm (3.0-in.) grid.

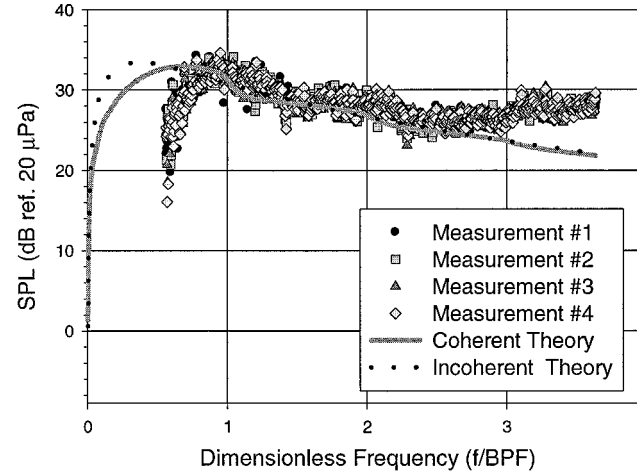

Fig. 4 Test case 2, predicted and measured SPLs: 10-bladed rotor located 61 cm (24 in.) downstream of 7.62-cm (3.0-in.) grid.

To isolate the rotor acoustic response, the background noise levels were power subtracted from the measured noise levels, taken with the rotor operating. Furthermore, a 3-dB discriminant was applied to ensure rejection of those frequency bands that were background dominated. The resulting data define the empirical rotor response to the grid-generated turbulence. These data were generated for both the 10-bladed and 4-bladed rotors at the test conditions defined in Tables 1 and 2, respectively. The measured 10-bladed acoustic response is compared to corresponding broadband noise predictions in Sec. IV.B. The measured response of both rotors is compared in Sec. IV.C.

B. Comparison Between Estimated and Measured 10-Bladed Response

Comparisons of the predicted broadband response and measured emissions from the 10-bladed rotor are presented in Figs. 4 and 5, respectively. Predictions of both the incoherent (uncorrelated) and coherent broadband response are plotted, where the degree of blade-to-blade correlation in the coherent response was accounted for by the summation gain, as defined in Sec. II.B. These data indicate that the estimated broadband levels agree very well with the measured data over the frequency range from the BPF to the third harmonic of the BPF. However, at low frequencies ($f <$ BPF), the measured data fall off sharply, whereas the predicted levels decay more slowly. This caused the predicted narrowband response (or haystacking) about the BPF to differ significantly from the measured values, which exhibited a more pronounced narrowband character. At the first and second harmonics of BPF, that is, 2BPF and 3BPF, the predicted narrowband response was much closer to the measured data, but still not quite as broad. At frequencies above the second harmonic ($f >$ 3BPF), the measured SPL diverged from the predicted levels,

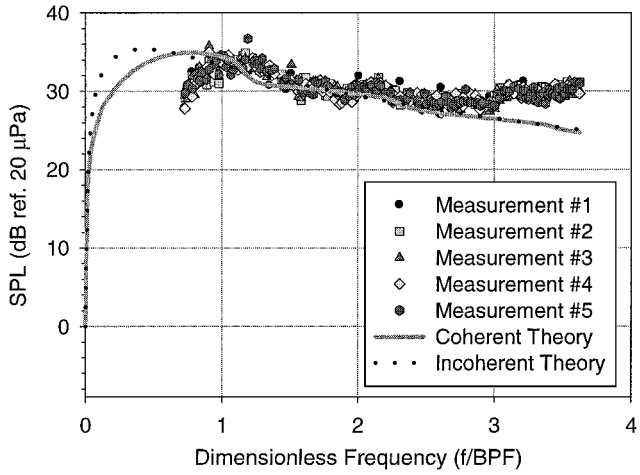

Fig. 5 Test case 2, predicted and measured SPLs: 10-bladed rotor located 61 cm (24 in.) downstream of 7.62-cm (3.0-in.) grid.

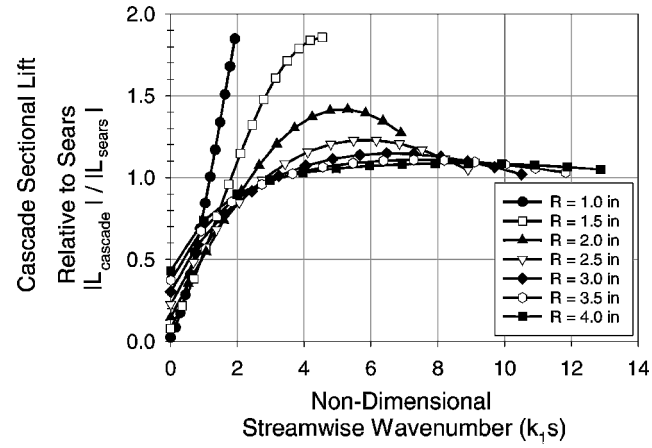

Fig. 6 Sectional lift response comparison: cascade geometry equivalent to 10-bladed rotor at specified radii.

suggesting the presence of an additional broadband source, which was not accounted for in the model. These trends were consistent for all test cases.

The relative agreement between the predicted broadband acoustic levels and the measured SPL over the middle frequency band (BPF $< f <$ 3BPF) indicates that the analysis presented in Sec. II.B, based on the semi-empirical turbulence model from part I of this paper,[1] successfully captured the incoherent portion of the rotor response to the grid-generated turbulence. As shown in Eq. (7), this suggests that the radial and streamwise components of the empirical turbulence model accurately represent the turbulent energy distribution with respect to these spatial directions. However, the differences in the predicted and measured narrowband features suggests that the analysis underestimated the degree of blade-to-blade correlation in the rotor response [the integral term in braces in Eq. (7)]. As modeled, this term depends on the tangential portion of the turbulence spectrum and the summation gain defined by Eq. (8). The former is a component of the empirical turbulence model, whereas the latter is an artifact of the blade-to-blade interaction geometry as modeled. It is not clear from these data which of these terms causes the underprediction of the narrowband response.

The enhanced acoustic production at high frequencies ($f >$ 3 BPF) was consistent with noise due to flow past the trailing edges of the blades. According to Blake,[3] "In short, ... subsonic acoustic sources important at trailing edges are generally caused by the turbulent boundary layer and wake flow generated by the lifting surface itself, rather than by the upstream turbulence." Such sources were not accounted for in the broadband prediction model, which assumed inviscid flow over the blades (see Sec. II.B). Furthermore, because these effects are associated with the turbulent length scales in the boundary-layer, trailing edge noise sources are generally broadband, at fairly high temporal frequencies. To investigate this possibility, the boundary-layer thickness at the trailing edge was estimated in terms of the temporal frequency, where trailing edge (TE) effects become important, f_{TE} (the frequency where the measured broadband levels diverge from the predicted levels) and the local convection velocity on the blade [as defined in Eq. (2)]:

$$\delta_{\mathrm{TE}} \approx V_c / 2\pi f_{\mathrm{TE}} \tag{9}$$

This approximation was applied to the empirical data presented in Figs. 4 and 5, assuming that the maximum trailing edge noise was generated at the blade tips, where the maximum convection velocity was achieved. The resulting empirical boundary layer thickness was $\delta_{\mathrm{TE}} \approx 3.4$ mm (0.13 in.). Because the rotor blades were thin ($t/c \approx 0.09$), a corresponding theoretical boundary-layer thickness was estimated, using Schlichting's expression for fully developed flow over a flat plate.[13] The result of this theoretical analysis was the same order of magnitude as the empirical approximation $\delta_{\mathrm{theory}} \approx 1$ mm (0.04 in.). This relative agreement suggests the differences between the measured and predicted sound levels at high frequencies were assessed to be TE effects.

Similarly, the disagreement at low frequencies was believed to be due to physical limitations of the relatively simple aerodynamic and acoustic response models. In particular, it was assumed in Sec. II.B that the rotor solidity was sufficiently small that the blade sections could be treated independently, rather than as a linear cascade of interacting airfoils. This assumption was equivalent to assuming infinite blade spacing ($b/c \to \infty$). However, previous investigators have shown that analyses based on isolated blades overpredict the sectional unsteady lift at low reduced frequencies ($k_1 c/2 \to 0$) (Ref. 3). Therefore, the overprediction of the response at low frequencies was characteristic of rotor solidity effects.

To investigate this possibility, a numeric aeroacoustic prediction model,[14] which was based on linear cascade theory, was used to estimate the unsteady lift response of the 10-bladed rotor blade section at a series of radial locations. These data were used to define a relative cascade effect parameter, nondimensionalizing the predicted cascade unsteady lift response with respect to the corresponding sears response, as shown in Fig. 6. These data support the suggestion that the discrepancies between the predicted and measured response at low frequencies were an artifact of ignoring rotor solidity effects in the theoretical model. However, note that both of these arguments are primarily anecdotal. Additional detailed analysis is required to determine conclusively the causes of the discrepancies at both high and low frequencies.

C. Comparison Between 10-Bladed and 4-Bladed Rotor Responses

In addition to the 10-bladed rotor response measurements, experiments were performed to determine the corresponding response characteristics of the 4-bladed rotor to the same ingested velocity field. The purpose of these tests was to contrast the 4-bladed response with that of the 10-bladed rotor, for the same turbulence grid. Consequently, the acoustic emissions from the 4-bladed rotor were measured for the same receiver/source geometry, at the same mean flow velocity and rotational speeds as those defined for the 10-bladed rotor test.

There were two principal differences between the two rotor geometries. One principal difference between the two rotor geometries was the blade spacing, which was nominally 9.4 cm (3.7 in.) for the 4-bladed rotor (at 75% of the tip radius), as compared to 4.6 cm (1.8 in.) for the 10-bladed rotor. In addition, the 4-bladed rotor chord varied with radial location, with a nominal geometric mean of 5.6 cm (2.2 in.), whereas the 10-bladed rotor had a constant 2.54-cm (1-in.) chord. Furthermore, the resulting advance coefficients were different for each rotor at a given flow velocity and rotation, because the diameter of the four-bladed rotor, 0.254 m (10 in.), was larger than that of the 10-bladed rotor, 0.203 m (8 in.). The purpose of the comparisons presented here is to highlight the differences in the character of the responses, and so only one test case is presented here. These data are for $\Omega = 3300$ rpm, which corresponds to BPF $= 220$ and $J = 0.91$ for

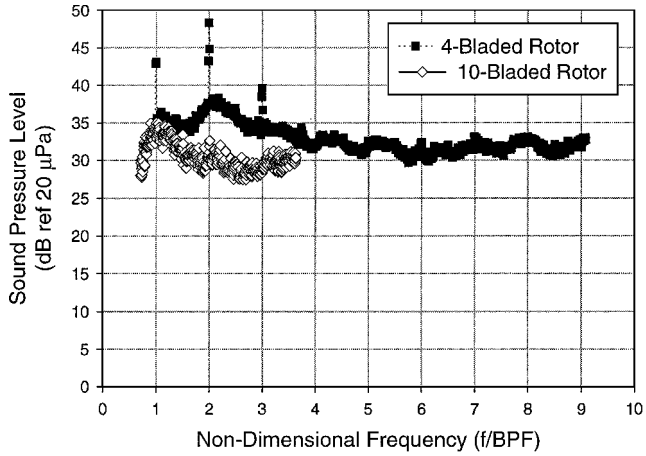

Fig. 7 Test case 3, measured SPL comparison, both rotors located 61 cm (24 in.) downstream of 7.62-cm (3.0-in.) grid microphone at $r_{mic} = 0.9$ m (36 in.); $\beta_{mic} = 45$ deg.

the four-bladed rotor. The measured SPL for both rotors at these conditions are shown in Fig. 7.

Consider the acoustic response characteristics of each rotor around the primary BPF and second harmonic. The four-bladed rotor response to the ingested turbulence field is dominated by tones at the BPF and its second harmonic. These signals are at least 10 dB above the broad-band levels. Additional tones are seen at the third and fourth harmonics, but these are only a few decibels above the broadband noise levels. In contrast, the measured response of the 10-bladed rotor was strictly broadband.

The tonal response of the four-bladed rotor to the 7.62 cm (3.0 in.), which was previously documented by both Scharpf[4] and Minniti et al.,[5] was due to the spatial inhomogeneity of the mean flowfield. As shown in part 1 of this paper,[1] the measured spatial mean velocity distribution behind the 7.62-cm (3.0-in.) turbulence grid exhibited a significant circumferential mode at $n = 4$.

To examine this hypothesis in a physical context, consider the acoustic response of the rotor to an ingested disturbance. Theoretical analyses[3] suggest that the amplitude of the rotor acoustic response to an ingested disturbance is strongly dependent on the correlation scales of that disturbance. The maximum radial and tangential correlation scales of the representative turbulence field were shown in part 1 of this paper to be approximately 2.3 cm (0.9 in.) and 1.15 cm (0.45 in.), respectively.[1] The corresponding rms turbulence amplitude u_{rms} is approximately 0.79 m/s (2.60 ft/s). In contrast, the circumferential mean velocity component at $n = 4$ was fairly weak, with a nominal amplitude of 0.15 m/s (0.5 ft/s). Although this excitation is considerably smaller than the rms turbulence amplitude, the four-bladed rotor is extremely sensitive to the temporal disturbance established by the periodic motion of the blades through the relatively weak spatial $n = 4$ mean velocity mode. In this case, the majority of each blade responds coherently to the mean flow disturbance. Consequently, the radial and tangential correlation scales for the mean flow inhomogeneity can be approximated by the blade span, 10.2 cm (4.0 in.), and the average geometric chord length 5.6 cm (2.2 in.). To assess the fidelity of this physical model, the measured broadband SPL for the four-bladed rotor about the BPF and 2 BPF (as indicated in Fig. 7) was used in conjunction with the rms turbulence amplitude and scales, to define a local empirical acoustic response function for the sound generated by the four-bladed rotor, due to a distributed velocity excitation over a given correlation area. When these empirical response functions were used, the expected SPL at BPF and 2 BPF, due to the $n = 4$ mean velocity mode, were predicted, assuming that the entire blade radiated coherently. The predicted levels at BPF and 2 BPF, were approximately 45 and 50 dB, which agreed very well with the measured tones of 43 and 48 dB, respectively.

Thus, the aeroacoustic sensitivity of the four-bladed rotor to the mean flow inhomogeneity was much greater than its sensitivity to the ingested turbulence field. However, the four-bladed rotor did respond to the broadband turbulence. The broadband sound levels were generated by the rotor sampling of the ingested turbulence. In contrast, the lack of tonal response at the BPF and harmonics in the measured SPL from the 10-bladed rotor suggested that the mean velocity field did not contain significant modal content at integral multiples of 10. Rather, the sound generated by the 10-bladed rotor was strictly broadband in nature, as would be expected for TIN. Note that the modal decomposition of the measured mean velocity field, presented in part 1 of this paper,[1] suggested that a small-amplitude component existed at $n = 10$. However, the lack of measured tones at BPF indicate that the apparent $n = 10$ component was an artifact of the processing.

Finally, the narrowband character of the 4-bladed rotor TIN about the BPF and 2 BPF, was different from the corresponding data for the 10-bladed rotor. The measured 10-bladed sound demonstrated that the amplitude of the narrowband response decays at higher harmonics, as predicted by both Blake[3] and Martinez.[9] However, the four-bladed SPL data demonstrated a significant narrowband response amplitude at 2 BPF, with virtually no narrowband response at BPF. The reason for this apparent discrepancy is not known at this time.

V. Conclusions

In part 1 of this paper, a detailed empirical definition of the ingested velocity field was defined. This velocity field consisted of a spatiotemporally varying turbulence field superimposed on an inhomogeneous mean velocity distribution. A three-dimensional semi-empirical, separable turbulence model was defined in terms of spatially averaged, measured turbulence characteristics. The mean velocity distribution was demonstrated to contain acoustically relevant circumferential modes for a four-bladed rotor.

The acoustic response of two rotor geometries, the 10-bladed rotor of Sevik[2] and the 4-bladed rotor of Scharpf[4] and Minniti et al.[5] to the grid-generated turbulence field were measured. In addition, theoretical estimates of the broadband sound emitted by the 10-bladed rotor were generated using spectral analysis techniques, based on the semi-empirical turbulence model. Comparisons between the predicted and measured sound indicated that the spectral techniques could accurately predict the broadband levels over the frequency range from BPF to 3BPF. However, the underprediction of narrowband response about the BPF in the predictions suggested that the degree of blade-to-blade correlation was underpredicted in the response model. This discrepancy suggests that improvements are needed in either the tangential component of the empirical turbulence model and/or the geometric model of blade–disturbance interaction, as shown in the summation gain defined in Eq. (8). However, the agreement of the overall broadband levels suggested that the rotor–turbulence interaction was accurately modeled with respect to the radial and streamwise directions. In addition, the theoretical model overpredicted the rotor response at low frequencies, which suggested that rotor solidity effects may be important for the 10-bladed rotor. Similarly, the high-frequency response was underpredicted, which suggested that the rotor acoustic response in this region may be dominated by TE noise.

Finally, comparisons between the measured sound generated by both rotor geometries demonstrated the relative importance of mean flow inhomogeneities and broadband turbulence on the rotor acoustic response. The tonal response of the four-bladed rotor indicated that the $n = 4$ circumferential mode of the mean flow was the dominant velocity feature of the ingested flowfield for that geometry, whereas the strictly broadband nature of the 10-bladed rotor response indicated that only the ingested turbulence was acoustically relevant.

Acknowledgments

This work was supported by the U.S. Navy, Office of Naval Research, located in Arlington, Virginia, under the following Contracts: N00014-97-1-0489, N00014-98-1-0217, and N00014-99-1-0284. The Program Manager was L. Patrick Purtell. This research was performed at the Hessert Center for Aerospace Research, Department of Aerospace and Mechanical Engineering, at the University of Notre Dame.

References

[1]Wojno, J. P., Blake, W. K., and Mueller, T. J., "Rotor Turbulence Ingestion Noise, Part 1: Experimental Characterization of Grid-Generated Turbulence," *AIAA Journal*, Vol. 40, No. 1, 2002, pp. 16–25.

[2]Sevik, M., "Sound Radiation from a Subsonic Rotor Subjected to Turbulence," NASA SP 304, 1971.

[3]Blake, W., *Mechanics of Flow Induced Sound and Vibration*, Wiley, New York, 1986, Chap. 12.

[4]Scharpf, D. F., "An Experimental Investigation of the Sources of Propeller Noise Due to Turbulence Ingestion," Ph.D. Dissertation, Dept. of Aerospace and Mechanical Engineering, Univ. of Notre Dame, Notre Dame, IN, Jan. 1993.

[5]Minniti, R. J., III, Blake, W. K., and Mueller, T. J., "Determination of Inflow Distortion Characteristics by Interpreting the Aeroacoustic Response of a Propeller Fan," *Proceedings of the 4th AIAA/CEAS Aeroacoustics Conference*, Vol. 1, Confederation of European Aerospace Societies, Toulouse, France, 1998, pp. 483–496.

[6]Martinez, R., "Asymptotic Theory of Broadband Rotor Thrust, Part I: Manipulations of Flow Probabilities for a High Number of Blades," *Journal of Applied Mechanics*, Vol. 63, March 1996, pp. 136–142.

[7]Wojno, J. P., "An Experimental Investigation of the Aeroacoustic Response of a Ten-Bladed Rotor Ingesting Grid-Generated Turbulence," Ph.D. Dissertation, Dept. of Aerospace and Mechanical Engineering, Univ. of Notre Dame, Notre Dame, IN, April 1999.

[8]Martinez, R., "Asymptotic Theory of Broadband Rotor Thrust, Part II: Analysis of the Right Frequency Shift of the Maximum Response," *Journal of Applied Mechanics*, Vol. 63, March 1996, pp. 143–148.

[9]Martinez, R., "Broadband Sources of Structure-Borne Noise for Propulsors in Haystacked Turbulence," *Computers and Structures*, Vol. 65, No. 3, 1997, pp. 475–490.

[10]Mueller, T. J., Scharpf, D. F., Batill, S. M., Strebinger, R. B., Sullivan, C. J., and Subramanian, S., "The Design of a Low-Noise, Low-Turbulence Wind Tunnel for Acoustic Measurements," AIAA Paper 92-3883, 1992.

[11]Subraminian, S., "Experimental and Computational Studies on Propeller Noise Due to Inflow Distortion," Ph.D. Dissertation, Dept. of Aerospace and Mechanical Engineering, Univ. of Notre Dame, Notre Dame, IN, May 1993.

[12]Figliola, R., and Beasley, D. E., *Theory and Design for Mechanical Measurements*, Wiley, New York, 1991, Chap. 5, p. 150.

[13]Schlichting, H., *Boundary Layer Theory*, McGraw–Hill, New York, 1979, p. 638.

[14]Atassi, H., and Hamad, G., "Sound Generated in a Cascade by Three-Dimensional Disturbances Convected in a Subsonic Flow," AIAA Paper 81-2046, Oct. 1981.

P. J. Morris
Associate Editor